# Spectral Analysis of Nonlinear Wave Forces

O.M.Boaghe, S.A.Billings, P.K.Stansby
Department of Automatic Control and Systems Engineering
University of Sheffield
Mappin Street, Sheffield S1 3JD
United Kingdom

Research Report No. 673

May 16, 1997

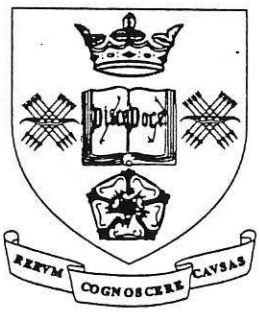


University of Sheffield



# Spectral Analysis of Nonlinear Wave Forces

O. M. Boaghe †, S. A. Billings †, P.K. Stansby ‡

May 16, 1997

† Department of Automatic Control and Systems Engineering, University of Sheffield, Po.Box-600, Mappin Street, S1 3JD, UK

‡ Hydrodynamics Research Group, School of Engineering, University of Manchester, Oxford Road, Manchester, M13 9PL, UK

**Abstract**

The spectral analysis of nonlinear wave forces is investigated based on the Morison equation and related models including the recently introduced Dynamic Morison model. An expression for the response power spectrum is initially derived in terms of the higher-order nonlinear frequency response functions and the spectrum of the input velocity. It is then shown how this can be evaluated for the Dynamic Morison model to yield an expression for the output power spectrum in terms of the coefficients of the time-domain differential equations and properties of the input. A comparison of the output spectra computed using traditional methods and the new expression of the response spectrum over several data sets is included. An interpretation of the Morison equation response spectrum is finally given.

## 1 Introduction

Spectral analysis is widely used in the study of wave forces and the safety assessment of offshore structures. The response spectral density is computed based on the linearised model or more recently by including a $u^3$ term to account for the $u|u|$ term in the Morison equation, where $u$ is flow velocity. However, recent results have shown that the Morison equation can be significantly improved by adding force history terms to yield the Dynamic Morison model. In the present study a new expression is derived for the output power spectrum of the Dynamic Morison model which explicitly reveals the dependence of this on the coefficients of the time-domain differential equations.

Initially the modelling of the nonlinear wave forces based on the Morison, Morison-Duffing, NARMAX and Dynamic Morison model are briefly discussed. The higher-order frequency response functions of the Dynamic Morison model are then derived as a function of the model coefficients. Substituting these into the power spectra yields, for the first time,

an explicit expression for the output power spectrum in terms of the coefficients of the Dynamic Morison nonlinear differential equations. A direct link between the time-domain model coefficients, properties of the input and the power spectrum is therefore established. This has important implications for future studies on the fatigue life computation and also on the analysis of the form and sensitivity of the spectrum in terms of the model parameters.

Spectra computed using the new formula are compared with spectra computed over five data sets refered to as Salford (Baker, 1994), De-Voorst and Christchurch Bay data (Stansby et al, 1992), to validate the new procedure. This study is concluded with a critical analysis of the Morison equation response spectrum.

# 2 Modelling nonlinear wave forces

A fundamental problem in the prediction of the nonlinear wave forces is the construction of accurate force models. Four main types of models are presented and briefly discussed in this section: the Morison equation, Morison-Duffing equation, NARMAX parametric models and Dynamic Morison models.

The traditional way of modelling wave forces is based on the Morison equation (Morison et al, 1950) which assumes that the force is composed of a linear combination of inertia and drag forces. This equation is used when the drag force is significant.

The Morison equation can be written as:

$$\begin{aligned} F(t) &= \frac{1}{4}\pi\rho D^2 C_m \frac{du(t)}{dt} + \frac{1}{2}\rho D C_d u(t)|u(t)| \\ &= K_i \frac{du(t)}{dt} + K_d u(t)|u(t)| \end{aligned} \tag{1}$$

where $F(t)$ is the force per unit axial length, $u(t)$ is the instantaneous flow velocity, $\rho$ is the water density and $D$ is the diameter. The drag and inertia coefficients $C_d$ and $C_m$ depend on the characteristics of the flow.

The Morison equation generally predicts the main trends in the measured data quite well, however some characteristics of the flow are not well represented. These can be revealed during a frequency domain analysis.

It is not possible to directly map the Morison equation into the frequency domain using the techniques of Volterra series due to the presence of the drag term $u(t)|u(t)|$ which has a discontinuous derivative. A necessary condition for the existence of the Volterra series is that all nonlinearities must be infinitely differentiable (Palm and Poggio, 1987). The drag term can however be approximated by a polynomial of the form:

$$u(t)|u(t)| = a_1 u(t) + a_3 u^3(t) + a_5 u^5(t) + \ldots \tag{2}$$

This approximation holds under the assumption that the input signal is a zero-mean Gaussian signal whose odd order moments are identically zero (Bendat and Piersol, 1986).

The approximated Morison equation, for nonlinearities in the input up to third order, is therefore given by:

$$F(t) = K_i \frac{du(t)}{dt} + K_{d1} u(t) + K_{d3} u^3(t) \tag{3}$$

The linear transfer function of the approximated Morison equation was computed by Swain et al (1996): $H_1(\omega_1) = K_{d1} + j\omega_1 K_i$. It is obvious from the linear transfer function that $\lim_{\omega_1 \to \infty} |H_1(\omega_1)| = \infty$, which means that when the cylinder is subject to a high frequency input wave of very small amplitude, it will experience an extremely high force. However, for most physical systems the gain of the system falls off as the frequency increases. It seems likely that the Morison equation requires modification and extension.

An extension of the Morison equation known as the Morison-Duffing equation was proposed by Stansby et al (1992) to predict wave forces in a variety of situations in which the history of vortex shedding can be a significant effect. The influence of vortex shedding was modelled by higher order and derivative terms in $F(t)$. Additional terms proportional to $F^2(t)$, $F^3(t)$, $\frac{dF(t)}{dt}$ and $\frac{d^2F(t)}{dt^2}$ were included, terms also present in the Duffing nonlinear oscillator equation. After some preliminary tests on U-tube data it became apparent that the $F^2(t)$ term could be discarded as insignificant. The model also showed a degree of improvement when the $F^3(t)$ term was replaced by one of the form $F(t)|F(t)|$. The form of the Morison-Duffing equation is thus:

$$\alpha_1 \frac{d^2F(t)}{dt^2} + \alpha_2 \frac{dF(t)}{dt} + \alpha_3 F(t)|F(t)| + F(t) = \frac{1}{4}\pi\rho D^2 C_m \frac{du(t)}{dt} + \frac{1}{2}\rho D C_d u(t)|u(t)| \tag{4}$$

Nonlinear wave force models can also be constructed using nonlinear system identification techniques based on the NARMAX approach. The NARMAX (Nonlinear Auto Regressive Moving Average with eXogenous inputs) model is an expansion of past inputs, outputs and noise terms (Leontaritis and Billings, 1985).

$$F(k) = f[F(k-1), \ldots, F(k-n_F), u(k-1), \ldots, u(k-n_u), e(k-1), \ldots, e(k-n_e)] + e(k) \tag{5}$$

$F(k)$, $u(k)$ and $e(k)$ are the discrete-time output, input and noise respectively at the time intervals $k$ and $f$ is a nonlinear rational or polynomial function. System identification based on this model consists of determining the model structure, followed by parameter estimation and model validation. Nonlinear wave force models were identified using the NARMAX model by Worden et al (1994).

The predictive performance of the estimated models were found to be better than the Morison equation but the models were difficult to interpret. Although identified NARMAX models are not necessarily unique for a particular data set, if they capture the underlying system characteristics all the models should exhibit the important dynamic features of the system. For example, if the NARMAX model represents the underlying system accurately it must reflect the unique linear and nonlinear frequency behaviour of the system.

Swain et al (1996) developed and discussed a new model structure, the Dynamic Morison equation, based on the frequency domain uniqueness of identified NARMAX models associated with nonlinear wave forces. The procedure employed to determine the model consisted of two stages: estimation of a discrete-time (NARMAX) model from sampled input-output data and computation of the generalised frequency response functions. Continuous time nonlinear differential equation models were then identified by curve fitting to the complex linear and higher order frequency response data using a weighted complex orthogonal estimator (Swain et al, 1996).

The continuous-time model is very similar to the Morison and Duffing-Morison equations and is referred to as the a Dynamic Morison equation:

$$\alpha_1 \frac{d^2F(t)}{dt^2} + \alpha_2 \frac{dF(t)}{dt} + F(t) = K_i \frac{du(t)}{dt} + K_{d1}u(t) + K_{d3}u(t)^3 \qquad (6)$$

The constants and coefficients associated with the Morison and Dynamic Morison models were identified for the Salford Cylinder, De-Voorst and Christchurch Bay data sets by Swain et al (1996) and are summarised in Table 1.

Table 1: Coefficients for Morison (3) and Dynamic Morison (6) continuous-time models (Swain et al, 1996)

| Data Set | Equation Type | $K_i$ | $K_{d1}$ | $K_{d3}$ | $\alpha_1$ | $\alpha_2$ |
|---|---|---|---|---|---|---|
| Salford Set 1 | Morison | 2.32 | 1.56 | 171.68 | - | - |
| | Dynamic Morison | 2.14 | 2.09 | 108.12 | 0.04 | 0.22 |
| Salford Set 2 | Morison | 2.12 | 1.39 | 208.40 | - | - |
| | Dynamic Morison | 2.08 | 1.99 | 116.44 | 0.04 | 0.22 |
| Salford Set 3 | Morison | 2.14 | 1.72 | 152.47 | - | - |
| | Dynamic Morison | 1.90 | 1.49 | 162.32 | 0.04 | 0.19 |
| Christchurch Bay Set | Morison | 148.67 | 54.33 | 32.02 | - | - |
| | Dynamic Morison | 171.14 | 23.00 | 23.25 | 0.27 | 0.56 |
| De-Voorst Set | Morison | 169.66 | 27.05 | 72.22 | - | - |
| | Dynamic Morison | 171.94 | 4.81 | 74.00 | 0.02 | 0.16 |

For the present analysis a third order NARMAX model was found to be sufficient to model all the relevant features of the data and hence the estimated continuous-time model incorporates nonlinear terms up to third degree. However, depending on the different experimental conditions, the nonlinear NARMAX model may contain higher-order nonlinear terms of the input. To accommodate these possibilities the Dynamic Morison equation can be rewritten as:

$$\alpha_1 \frac{d^2F(t)}{dt^2} + \alpha_2 \frac{dF(t)}{dt} + F(t) = \frac{1}{4}\pi\rho D^2 C_m \frac{du(t)}{dt} + \frac{1}{2}\rho D C_d u(t)|u(t)| \qquad (7)$$

Spectral analysis derived for the Morison equation, the NARMAX model and the Dynamic Morison equation, for all five data sets analysed in Swain et al (1996) will be

studied in the next section. New characteristics of the Morison equation can be revealed and interpreted by using the estimated response spectrum.

# 3 Spectral analysis of nonlinear wave forces

Frequency domain analysis is important in wave force analysis because it provides a direct link to the fatigue life of offshore structures. There are several ways in which spectral analysis can be performed. Spectral estimates can be obtained from measured input and output signals, from a predicted output signal via an identified continuous-time differential equation, or from the predicted output spectrum via the nonlinear frequency response functions. The latter case is particularly informative because an analytic expression for the power spectral density can be obtained, as a function of the nonlinear frequency response functions and the parameters of the system model.

The application of spectral analysis to nonlinear wave forces is directly dependent on the type of input signal applied to the system, that is deterministic or random signals. For deterministic input signals, the response power spectrum has been derived, for example by Worden et al (1994). In real situations the input signal is random and a new approach has to be adopted. The response power spectrum for nonlinear wave forces is derived in the following sections, when random input signals are applied to the system.

## 3.1 Response power spectrum estimation for nonlinear systems - an overview

Since all the models discussed above are nonlinear, methods of analysing nonlinear models in the frequency domain will be briefly discussed below.

The traditional description of nonlinear systems has been based on the Volterra series. Volterra (1959) showed that every continuous functional $F(u)$ in the field of continuous functionals can be represented by the Volterra expansion:

$$F(u) = \sum_{n=0}^{\infty} F_n[u] \tag{8}$$

in which $F_n[\cdot]$ is a regular homogeneous functional of the form:

$$F_n[t] = \int_{-\infty}^{\infty} \dots \int_{-\infty}^{\infty} h_n(\tau_1, \tau_2, \dots, \tau_n) u(t-\tau_1) u(t-\tau_2) \dots u(t-\tau_n) d\tau_1 d\tau_2 \dots d\tau_n \tag{9}$$

The index $n$ is the degree of the functional. The series is called convergent if a definite value of the functional corresponds to every function $u(t)$.

The $n$th-order kernel of (9), $h_n(\tau_1, \tau_2, \dots, \tau_n)$ is often referred to as a nonlinear impulse response of order $n$. The Fourier transform of $h_n(\cdot)$ is called the nonlinear transfer function or generalised frequency response function of order $n$:

$$H_n(\omega_1,\omega_2,\ldots,\omega_n) = \int_{-\infty}^{\infty}\cdots\int_{-\infty}^{\infty} h_n(\tau_1,\tau_2,\ldots,\tau_n)exp(-j(\omega_1\tau_1+\omega_2\tau_2 + \ldots+\omega_n\tau_n))d\tau_1 d\tau_2\ldots d\tau_n \quad (10)$$

The power spectral density for a nonlinear system was derived by Rugh (1981), with a real, stationary, zero-mean and Gaussian input and is applied below to the nonlinear wave forces case.

When $u(t)$ is a real random process, the expected value of the output is expressed as (Rugh, 1981):

$$\begin{aligned} E[F_n(t)] &= \int_{-\infty}^{\infty}\cdots\int_{-\infty}^{\infty} h_n(\tau_1,\ldots,\tau_n)E[u(t-\tau_1)\ldots u(t-\tau_n)]d\tau_1\ldots d\tau_n \\ &= \int_{-\infty}^{\infty}\cdots\int_{-\infty}^{\infty} h_n(\tau_1,\ldots,\tau_n)R_{uu}^{(n)}(t-\tau_1,\ldots t-\tau_n)d\tau_1\ldots d\tau_n \end{aligned} \quad (11)$$

where the $n$-th order autocorrelation of the input $u(t)$ is defined by:

$$R_{uu}^{(n)}(t_1,\ldots,t_n) = E[u(t_1),\ldots,u(t_n)] \quad (12)$$

From equation (11) the expected value of the output depends on the $n$th-order input autocorrelation. In other words, as $n$ increases more statistical information about the input is needed to characterise the expected value of the output.

Initially the power spectral density is computed for the $n$-order output in equation (8). The complete expression for the output spectrum is then constructed based on this result. The multi-variable output autocorrelation $R_{yy}(t_1,\ldots,t_{2n})$ is defined as (Rugh, 1981):

$$R_{FF}(t_1,\ldots,t_{2n}) = \int_{-\infty}^{\infty}\cdots\int_{-\infty}^{\infty} h_n(\tau_1,\ldots,\tau_n)h_n(\tau_{n+1},\ldots,\tau_{2n}) R_{uu}^{(2n)}(t_1-\tau_1,\ldots,t_{2n}-\tau_{2n})d\tau_1\ldots d\tau_{2n} \quad (13)$$

The response power spectrum of the output $F_n(t)$ can then be computed as a function of order $2n$ of the input autocorrelation function:

$$S_{FF}^{(2n)}(\omega_1,\ldots,\omega_{2n}) = H_n(\omega_1,\ldots,\omega_n)H_n(\omega_{n+1},\ldots,\omega_{2n})S_{uu}^{(2n)}(\omega_1,\ldots,\omega_n) \quad (14)$$

When a stationary input is applied to a stationary $n$th-order system, the usual time-shift argument shows that the output process is stationary (Chrysostomos, Petropulu,

1993). Thus, for a stationary random input signal the output autocorrelation and power spectral density can be expressed as a function of a single variable (Rugh, 1981):

$$\begin{aligned} S_{FF}(\omega) &= \frac{1}{(2\pi)^{2n-1}} \int_{-\infty}^{\infty} \cdots \int_{-\infty}^{\infty} S_{FF}^{(2n)}(\gamma_1, \ldots, \gamma_{2n}) \delta(\omega - \gamma_1 - \ldots - \gamma_n) d\gamma_1 \ldots d\gamma_{2n} = \\ &= \frac{1}{(2\pi)^{2n-1}} \int_{-\infty}^{\infty} \cdots \int_{-\infty}^{\infty} H_n(\gamma_1, \ldots, \gamma_n) H_n(\gamma_{n+1}, \ldots, \gamma_{2n}) S_{uu}^{(2n)}(\gamma_1, \ldots, \gamma_{2n}) \\ &\quad \delta(\omega - \gamma_1 - \ldots - \gamma_n) d\gamma_1 \ldots d\gamma_{2n} \end{aligned} \tag{15}$$

To achieve further simplification it is assumed that the input is a real, stationary random process with zero-mean and a Gaussian distribution. In this case the higher-order autocorrelations of the input process can be expressed in terms of the 2nd-order moments and hence the $n$th-order autocorrelation function can be written as (Rugh, 1981):

$$R_{uu}^{(n)}(t_1, \ldots, t_n) = \begin{cases} \sum_p \prod_{j,k}^{n} R_{uu}(t_j - t_k), & n \text{ even} \\ 0, & n \text{ odd} \end{cases} \tag{16}$$

where $\prod_{j,k}^{n}$ is a product over a set of $n/2$ (unordered) pairs of integers from $1, 2, \ldots, n$ and $\sum_p$ is a sum over all $(n-1)(n-3)\ldots(1) = \frac{n!}{(n/2)!2^{n/2}}$ such products.

The corresponding power spectral density is then:

$$S_{uu}^{(n)}(\omega_1, \ldots, \omega_n) = \begin{cases} (2\pi)^{n/2} \sum_p \prod_{j,k}^{n} S_{uu}(\omega_j) \delta(\omega_j + \omega_k), & n \text{ even} \\ 0, & n \text{ odd} \end{cases} \tag{17}$$

The response power spectrum is therefore:

$$\begin{aligned} S_{FF}(\omega) &= \frac{1}{(2\pi)^{n-1}} \sum_p \int_{-\infty}^{\infty} \cdots \int_{-\infty}^{\infty} H_n(\gamma_1, \ldots, \gamma_n) H_n(\gamma_{n+1}, \ldots, \gamma_{2n}) \\ &\quad \delta(\omega - \gamma_1 - \ldots - \gamma_n) \prod_{j,k}^{2n} S_{uu}(\gamma_j) \delta(\gamma_j + \gamma_k) d\gamma_1 \ldots d\gamma_{2n} \end{aligned} \tag{18}$$

Rewriting equation (8) as:

$$F(t) = \sum_{n=1}^{\infty} F_n(t) \tag{19}$$

then for a real random input the output autocorrelation is (Rugh, 1981):

$$R_{FF}(t_1,t_2) = E[F(t_1)F(t_2)] = \sum_{n=1}^{\infty}\sum_{m=1}^{\infty} E[F_n(t_1)F_m(t_2)] = \sum_{n=1}^{\infty}\sum_{m=1}^{\infty} R_{F_nF_m}(t_1,t_2) \tag{20}$$

and the output power spectrum is the Fourier transform of the autocorrelation:

$$S_{FF}(\omega_1,\omega_2) = F(\sum_{n=1}^{\infty}\sum_{m=1}^{\infty} R_{F_nF_m}(t_1,t_2)) = \sum_{n=1}^{\infty}\sum_{m=1}^{\infty} S_{F_nF_m}(t_1,t_2) \tag{21}$$

In the case of a real, stationary, zero-mean, Gaussian input signal, with a power spectral density $S_{uu}(\omega)$, the partial output spectrum is $S_{F_nF_m} = 0$, when $n+m$ is odd, and when $n+m$ is even (Rugh, 1981):

$$\begin{aligned} S_{F_nF_m}(\omega) &= \frac{1}{(2\pi)^{(n+m-2)/2}} \sum_{p} \int_{-\infty}^{\infty} \dots \int_{-\infty}^{\infty} H_n(\gamma_1,\dots,\gamma_n) H_m(\gamma_{n+1},\dots,\gamma_{n+m}) \\ &\quad \delta(\omega-\gamma_1-\dots-\gamma_n) \prod_{j,k}^{n+m} S_{uu}(\gamma_j)\delta(\gamma_j+\gamma_k) d\gamma_1 \dots d\gamma_{n+m} \end{aligned} \tag{22}$$

## 3.2 Response power spectrum estimation for wave forces

The models presented in section 2 have a third-order nonlinearity, and therefore the response spectrum formula (22) for wave forces is based on the nonlinear frequency response functions up to third order. By applying equation (22) for a third-order nonlinear system, the output power spectrum is given as:

$$\begin{aligned} S_{FF}(\omega) &= H_1(\omega)H_1(-\omega)S_{uu}(\omega) + \frac{3}{2\pi} H_1(\omega)S_{uu}(\omega) \int_{-\infty}^{\infty} H_3(-\omega,\gamma,-\gamma)S_{uu}(\gamma)d\gamma + \\ &+ \frac{3}{2\pi} H_1(-\omega)S_{uu}(\omega) \int_{-\infty}^{\infty} H_3(\omega,\gamma,-\gamma)S_{uu}(\gamma)d\gamma + \\ &+ \frac{1}{2\pi}\delta(\omega) \int_{-\infty}^{\infty}\int_{-\infty}^{\infty} H_2(\gamma_1,-\gamma_1)H_2(\gamma_2,-\gamma_2)S_{uu}(\gamma_1)S_{uu}(\gamma_2)d\gamma_1 d\gamma_2 + \\ &+ \frac{1}{\pi} \int_{-\infty}^{\infty} H_2(\omega-\gamma,\gamma)H_2(-\omega+\gamma,-\gamma)S_{uu}(\gamma)S_{uu}(\omega-\gamma)d\gamma + \\ &+ \frac{6}{(2\pi)^2} \int_{-\infty}^{\infty}\int_{-\infty}^{\infty} H_3(\omega-\gamma_1-\gamma_2,\gamma_1,\gamma_2)H_3(-\omega+\gamma_1+\gamma_2,-\gamma_1,-\gamma_2) \\ &\quad S_{uu}(\omega-\gamma_1-\gamma_2)S_{uu}(\gamma_1)S_{uu}(\gamma_2)d\gamma_1 d\gamma_2 + \\ &+ \frac{9}{(2\pi)^2} S_{uu}(\omega) \int_{-\infty}^{\infty}\int_{-\infty}^{\infty} H_3(\omega,\gamma_1,-\gamma_1)H_3(-\omega,\gamma_2,-\gamma_2) \\ &\quad S_{uu}(\gamma_1)S_{uu}(\gamma_2)d\gamma_1 d\gamma_2 \end{aligned} \tag{23}$$

This expression can be simplified if it is assumed that $H_2(\omega_1, \omega_2) = 0$ for nonlinear wave forces and if the symmetry properties available for the input spectrum $S_{uu}$ and the transfer functions are considered. Since the properties of spectral conjugation hold for the nonlinear transfer function

$$H_n^*(\omega_1, \ldots, \omega_n) = H_n(-\omega_1, \ldots, -\omega_n) \tag{24}$$

equation (23) then reduces to:

$$\begin{aligned} S_{FF}(\omega) &= |H_1(\omega)|^2 S_{uu}(\omega) + \frac{3}{2\pi} H_1(\omega) S_{uu}(\omega) \int_{-\infty}^{\infty} H_3(-\omega, \gamma, -\gamma) S_{uu}(\gamma) d\gamma + \\ &+ \frac{3}{2\pi} H_1(-\omega) S_{uu}(\omega) \int_{-\infty}^{\infty} H_3(\omega, \gamma, -\gamma) S_{uu}(\gamma) d\gamma + \\ &+ \frac{6}{(2\pi)^2} \int_{-\infty}^{\infty} \int_{-\infty}^{\infty} |H_3(\omega - \gamma_1 - \gamma_2, \gamma_1, \gamma_2)|^2 \\ &\quad S_{uu}(\omega - \gamma_1 - \gamma_2) S_{uu}(\gamma_1) S_{uu}(\gamma_2) d\gamma_1 d\gamma_2 + \\ &+ \frac{9}{(2\pi)^2} S_{uu}(\omega) \int_{-\infty}^{\infty} \int_{-\infty}^{\infty} H_3(\omega, \gamma_1, -\gamma_1) H_3(-\omega, \gamma_2, -\gamma_2) \\ &\quad S_{uu}(\gamma_1) S_{uu}(\gamma_2) d\gamma_1 d\gamma_2 \end{aligned} \tag{25}$$

Having determined an expression for the power spectral density, the first and third order transfer functions $H_1(\omega)$ and $H_3(\omega_1, \omega_2, \omega_3)$ should be determined and substituted in equation (25). Consider the Dynamic Morison model (6) developed by Swain et al (1996). By applying the probing method developed by Peyton-Jones and Billings (1990) to the continuous-time differential equation (6), the nonlinear frequency response functions can be expressed explicitly in terms of the continuous-time model coefficients as:

$$\begin{aligned} H_1(\omega) &= \frac{K_{d1} + K_i(j\omega)}{1 - \alpha_2(j\omega) - \alpha_1(j\omega)^2} \\ H_2(\omega_1, \omega_2) &= 0 \\ H_3(\omega_1, \omega_2, \omega_3) &= \frac{K_{d3}}{1 - \alpha_2(j\omega_1 + j\omega_2 + j\omega_3) - \alpha_1(j\omega_1 + j\omega_2 + j\omega_3)^2} \end{aligned} \tag{26}$$

The transfer function expressions (26) can now be substituted into (25) and the response spectrum determined as:

$$S_{FF}(\omega) = S_{uu}(\omega) \frac{|K_{d1} + K_i(j\omega)|^2}{|1 - \alpha_2(j\omega) - \alpha_1(j\omega)^2|^2} + \frac{6}{2\pi} S_{uu}(\omega) \frac{K_{d1} K_{d3}}{(1 + \alpha_1\omega^2)^2 + (\alpha_2\omega)^2} \int_{-\infty}^{\infty} S_{uu}(\gamma) d\gamma$$

$$+ \quad \frac{6}{(2\pi)^2}\frac{|K_{d3}|^2}{|1-\alpha_2 j\omega+\alpha_1\omega^2|^2}\int_{-\infty}^{\infty}\int_{-\infty}^{\infty} S_{uu}(\omega-\gamma_1-\gamma_2)S_{uu}(\gamma_1)S_{uu}(\gamma_2)d\gamma_1 d\gamma_2 +$$

$$+ \quad \frac{9}{(2\pi)^2}S_{uu}(\omega)\frac{|K_{d3}|^2}{|1-\alpha_2 j\omega+\alpha_1\omega^2|^2}\left(\int_{-\infty}^{\infty} S_{uu}(\gamma_1)d\gamma_1\right)^2 \qquad (27)$$

It should be emphasized that the response spectrum is computed based on the $n$th-order input spectrum, which has been expressed as a function of the first order input spectrum $S_{uu}(\omega)$ in equation (17), when the input is a real, stationary, zero-mean and Gaussian signal.

The significance of the expressions in equations (25) and (26) is that for the first time the power spectral density of nonlinear wave force models has been expressed in a form which explicitly shows how the $PSD$ (power spectral density) depends on the model coefficients, in the case of a real, stationary, zero-mean and Gaussian input signal. These results provide significant insight into the operation of these systems and it is relatively easy to apply a similar analysis to other nonlinear systems.

The results which were obtained by applying the probing method to the continuous-time differential equations, which define the system dynamics, are given in equation (25) and (26). However the estimation procedure can only be applied for continuous-time differential equations, with no discontinuities, that is, in the case of nonlinear wave forces, only for a polynomial approximation of the drag term $u(t)|u(t)|$.

# 4 Spectral analysis performed on a fixed cylinder

Wave force data from a variety of systems have been modelled by Swain et al (1996). The data sets consisted of velocities and forces for three different rectangular wave spectra for a fixed cylinder, obtained from the University of Salford, forces and velocities measured on the Christchurch Bay Tower and a data set from the De Voorst facility at Delft Hydraulics.

In this section spectral analysis will be performed on the three model types: the Morison equation, the NARMAX parametric model and the Dynamic Morison equation (Swain et al, 1996). In each case the spectral estimates will be computed using two approaches. Both are based on the traditional methods of computing the spectral density but the first operates on the measured output signal and the second on the output produced by simulating the identified differential equation.

The response power spectrum will be estimated for Morison and Dynamic Morison equations and an example of fatigue life computation based on this estimates will be presented. Finally a comparison between Morison and Dynamic Morison power spectra will be made.

## 4.1 Spectral analysis of the time domain models

The power spectral density was computed for the measured output signal (the wave force) and for the output signal computed by simulating the identified continuous-time differential equations presented in Table 1. In all cases the input was a narrow band random stationary signal. The Welch non-parametric method (Proakis et al, 1992) was applied to the time sequences in order to find the power spectral density.

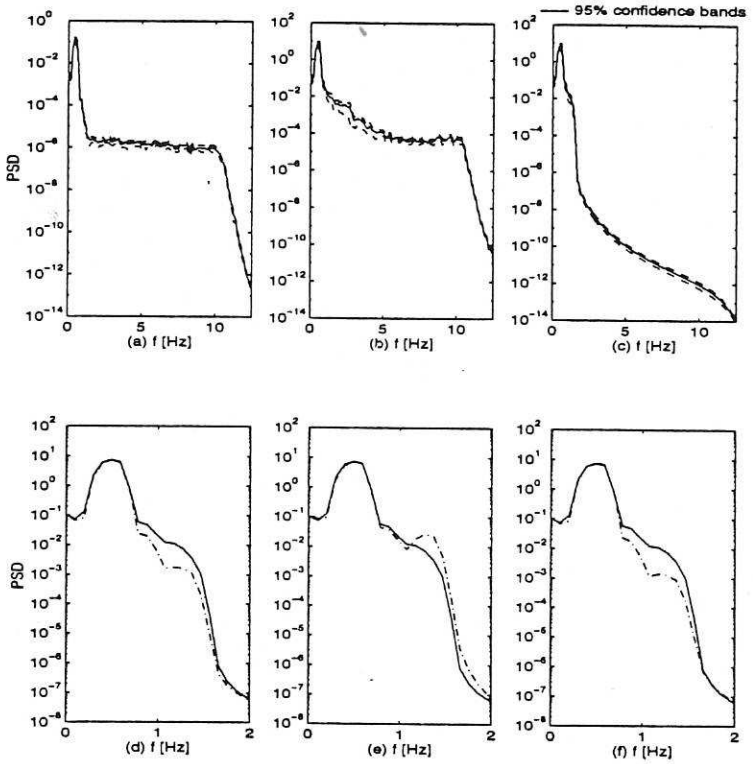


Figure 1: Power spectral density computed for the Salford Data Set 1: (a) Measured input data; (b) Measured output data; (c) Smooth output data; (d) NARMAX (dashed) and smooth output (solid) data; (e) Morison (dashed) and smooth output (solid) data; (f) Dynamic Morison (dashed) and smooth output (solid) data.

The results obtained for all five data sets are presented in Figures 1-5. The original input and output and the smooth output spectra are represented in the Figures 1-5 (a)-(c), where the dashed lines are 95% confidence bands. The confidence bands represent a precise measure of the quality of the spectrum estimate and are computed using the method presented in Wellstead (1986). The dashed lines in the Figures 1-5 (d)-(f) are the spectra computed for NARMAX, Morison and Dynamic Morison models, while the solid lines in the same figures represent the smooth original output spectrum. The signals are presented on a full scale in the Figures 1-5 (a)-(c) and only on the range relevant for the cubic nonlinearity in the Figures 1-5 (d)-(f).

In order to investigate the differences between these spectra, a nonlinear smoothing operation was applied to the high frequency bands of the original output signal. This has the effect of reducing the component of the signal which is produced by white noise. In

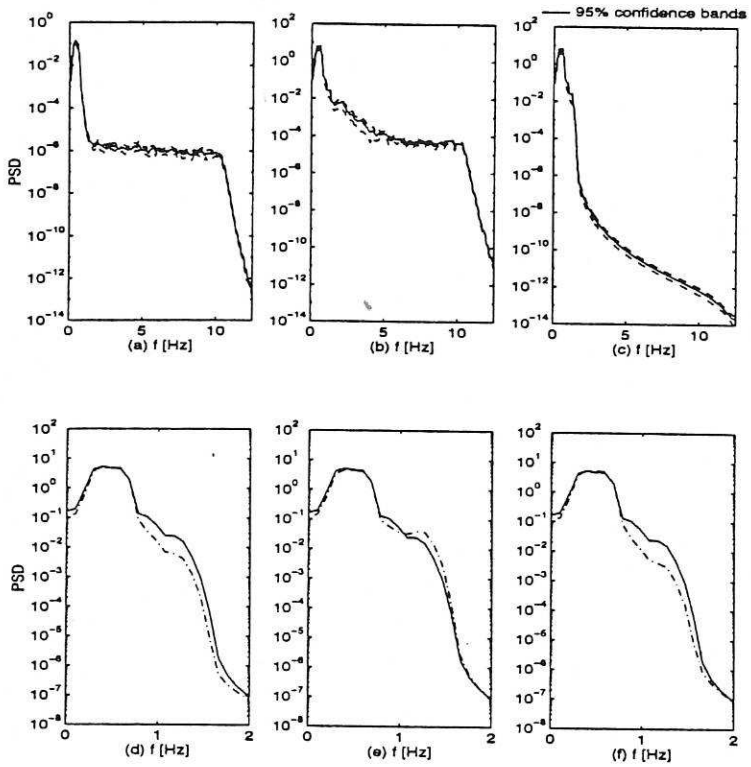


Figure 2: Power spectral density computed for the Salford Data Set 2: (a) Measured input data; (b) Measured output data; (c) Smooth output data; (d) NARMAX (dashed) and smooth output (solid) data; (e) Morison (dashed) and smooth output (solid) data; (f) Dynamic Morison (dashed) and smooth output (solid) data.

all subsequent data sets the output signal will be smoothed to remove the noise and both spectra from the original and smoothed signals will be presented.

In Figures 1-5 (d)-(f) the spectrum of the smooth measured output (Figure 1-5 (c)) is used as a reference and it should be compared with spectra for all three models (Figure 1-5 (d)-(f)). By analysing the graphs, it can be observed that the NARMAX (Figure 1-5 (d)) and the Dynamic Morison (Figure 1-5 (f)) models are almost identical in terms of spectrum shape. This fact is a new confirmation of the Dynamic Morison identification procedure, presented by Swain et al (1996).

The spectrum of the smoothed output shown in 1-5 (c) compares well with the spectrum produced by the noise free outputs generated from the NARMAX and Dynamic Morison equation models. The slight difference between the original output spectrum and the NARMAX estimated output spectrum corresponds to the noise model detected by the orthogonal-least-squares algorithm. The NARMAX output in Figures 1-5 (d) is noise free, while the original output 1-5 (b) includes coloured noise effects.

The NARMAX model (5) was validated using higher-order correlation tests. The correlation tests hold if the prediction error sequence $e(k)$ in (5) is reduced to an unpredictable sequence. This will be achieved and the estimates will be unbiased if the correlated noise is correctly accommodated in the identified noise model (Korenberg et al, 1988).

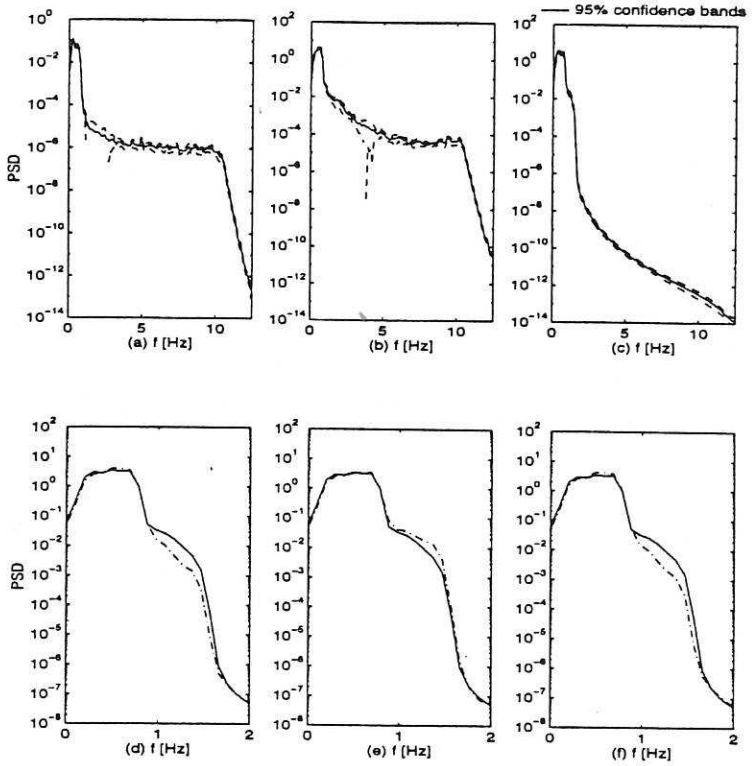


Figure 3: Power spectral density computed for the Salford Data Set 3: (a) Measured input data; (b) Measured output data; (c) Smooth output data; (d) NARMAX (dashed) and smooth output (solid) data; (e) Morison (dashed) and smooth output (solid) data; (f) Dynamic Morison (dashed) and smooth output (solid) data.

The Morison spectrum is also different from the measured output spectrum. The difference is caused by the Morison model which cannot capture the dynamics of the nonlinear system. As discussed by Swain et al (1996), the Morison model is likely to be inappropriate at high frequency components of the input signal, where the Morison model introduces additional spectral components which are not present in the smoothed output spectrum and which appear to be spurious. This provides further evidence that the NARMAX and Dynamic Morison models are a more appropriate fit to the underlying system.

## 4.2 Spectral analysis via the frequency transfer functions

The response spectra can also be computed by using the results in section 3.2. This consists of mapping the Dynamic Morison differential equation models from Table 1 directly into the frequency domain using equation (27).

The result of this analysis for all the data sets is summarised in Figure 6, where the spectra obtained analytically from equation (22) (dash-dot lines) are compared to the spectra obtained by simulating the Dynamic Morison differential equation in the time domain (solid lines).

A measure of comparison between the power spectral density curves can be provided

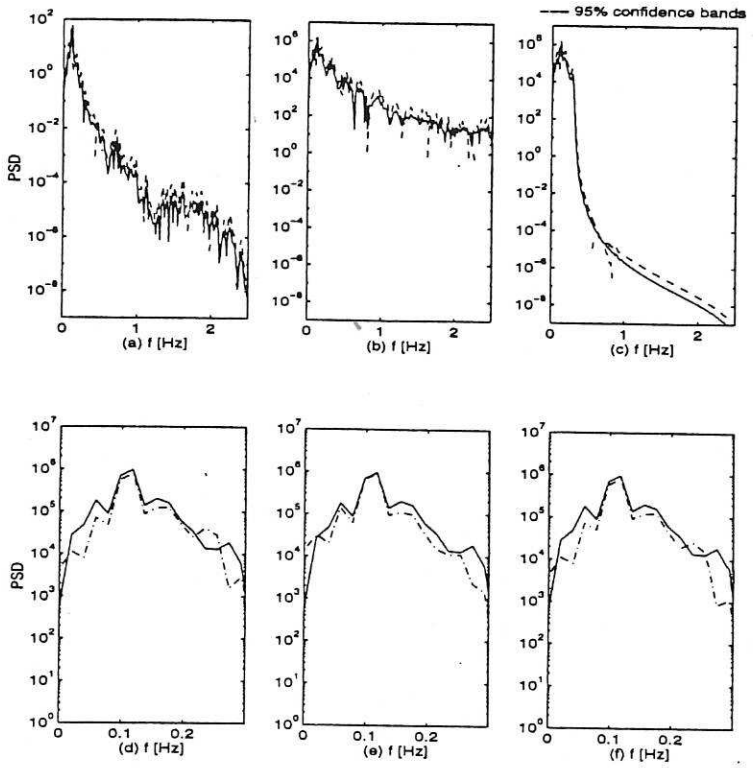


Figure 4: Power spectral density computed for the Christchurch Bay Data Set: (a) Measured input data; (b) Measured output data; (c) Smooth output data; (d) NARMAX (dashed) and smooth output (solid) data; (e) Morison (dashed) and smooth output (solid) data; (f) Dynamic Morison (dashed) and smooth output (solid) data.

by computing the $R$ and $NMSE$ values defined below. $NMSE$ and $R$ values have been computed for all the data sets and the results are presented in Table 2. The $NMSE$ is given by:

$$NMSE = \sqrt{\frac{\sum(S_{\hat{F}\hat{F}}(k) - S_{FF}(k))^2}{\sum(S_{FF}(k) - \bar{S}_{FF}(k))^2}} \tag{28}$$

where $S_{\hat{F}\hat{F}}(k)$ is the spectrum computed by simulating one of the three models presented in Table 1, $S_{FF}(k)$ is the spectrum computed from the measured output and $\bar{S}_{FF}(k)$ is the mean value of the spectrum for the measured output.

The average power $P_F$ in the signal spectra can also be considered.

$$P_F = E[S_{FF}] = \frac{1}{N}\sum S_{FF} \tag{29}$$

The normalised difference between the average power of the measured output and the computed output can then be computed as:

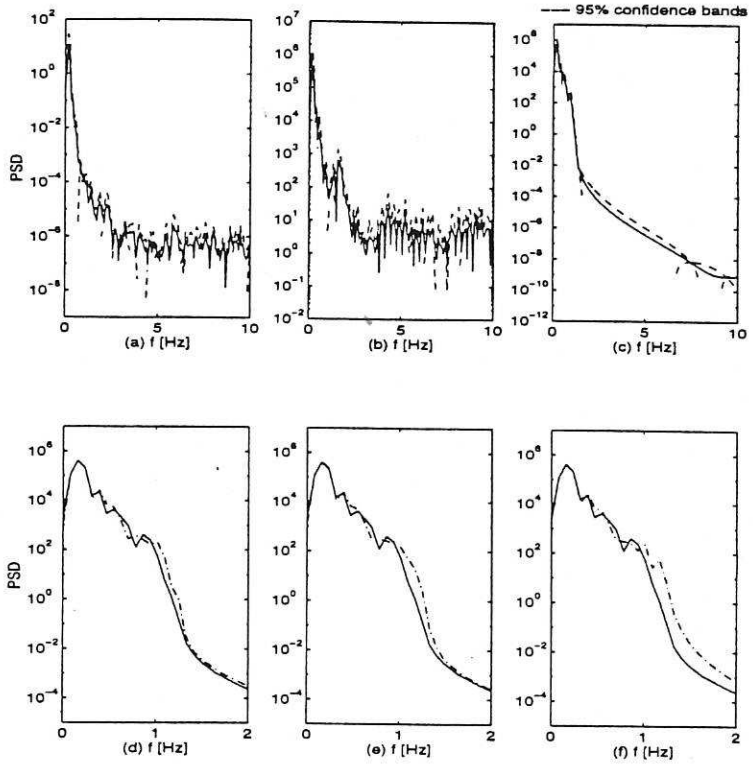


Figure 5: Power spectral density computed for the De-Voorst Data Set: (a) Measured input data; (b) Measured output data; (c) Smooth output data; (d) NARMAX (dashed) and smooth output (solid) data; (e) Morison (dashed) and smooth output (solid) data; (f) Dynamic Morison (dashed) and smooth output (solid) data.

$$R = \frac{S_{FF} - S_{\hat{F}\hat{F}}}{S_{FF}} \tag{30}$$

The accuracy of the estimate $S_{FF}$ is directly dependent on the input spectrum estimate $S_{uu}$. The estimate $S_{uu}$ was obtained for 8192 samples samples of the measured input and the Welch method of spectrum estimation assures an unbiased and very accurate estimate.

The processing time for the method based on equation (27) is determined by the 3rd-order convolution of the input spectrum $S_{uu}$ in equation (27) which requires an exponential computation time. Therefore a trade-off between accuracy and processing time was adopted. However, a small number of samples (128 in Figure 6) should not affect the accuracy of the estimate $S_{FF}$, providing the input spectrum estimate $S_{uu}$ is sufficiently accurate.

The advantage of using equation (25) or (27) is that the dependence of the spectral density on the model structure and coefficients is transparent. It is therefore very easy to visualise what a change in the model terms, the nonlinearity, the coefficients or the input spectrum will have on the power spectrum and to assess the sensitivity to these effects. A similar insight can also be gained for the fatigue life computation which is based on the

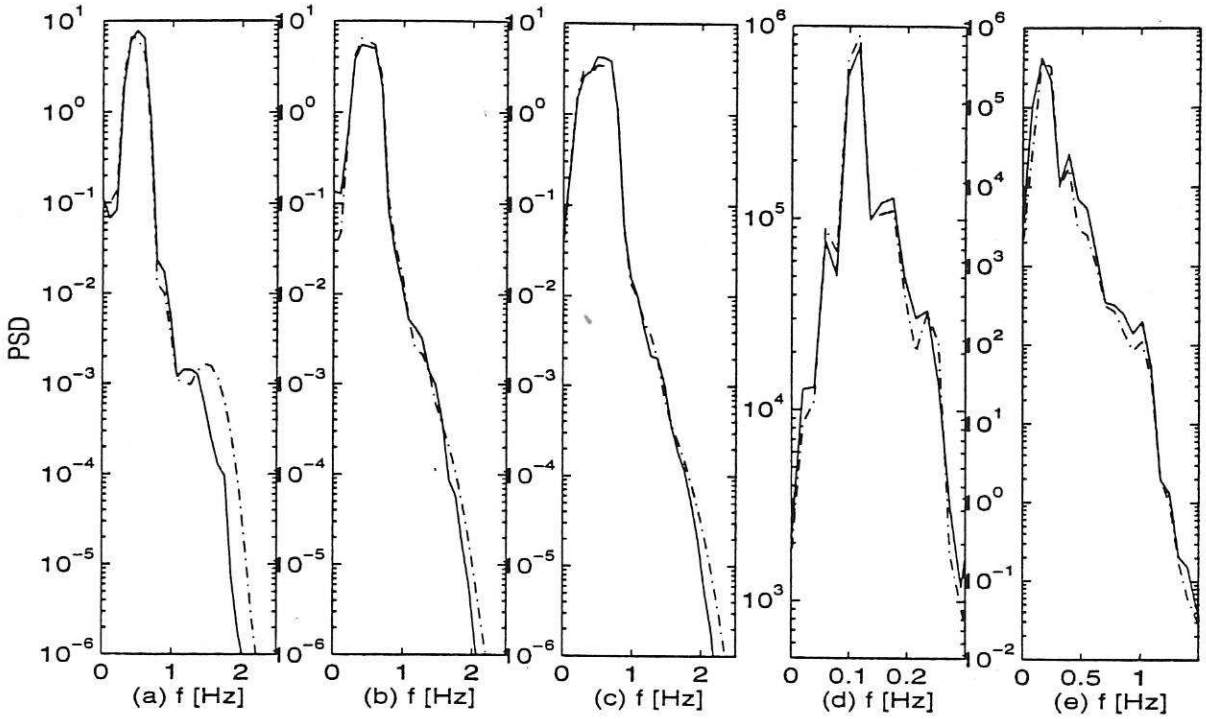


Figure 6: Power spectral density estimated for: (a) Salford Data Set 1; (b) Salford Data Set 2; (c) Salford Data Set 3; (d) Christchurch Bay Data Set; (e) De-Voorst Data Set

The solid lines represent the spectra from the Dynamic Morison equation calculated by standard methods, the dashed lines show the estimates obtained using equation (27).

response spectrum estimate and which will be discussed in the next section.

## 4.3 Application to fatigue life computation

The Morison and Dynamic Morison equations are compared in this section in terms of estimated fatigue life. Consider the problem of finding the expected fatigue life in years of the fixed cylinder subjected to random waves, used in the Salford experiment (Data Set 1), based on the estimated power spectrum of the wave force.

The problem is simplified and uniform loading considered, given the force measured on the sleeve, along the span. The stress at the support end of the cylinder is proportional to force: $S = k \times F$, where $k$ is a function of cylinder geometry, material and support. Here the constant $k$ is chosen arbitrarily to give a fatigue life of about 50 years.

The assessment of the fatigue life can be performed by using the so called S-N approach (British Standards Institution, 1980). This method, currently in general use, relies on empirically derived relationships between stress ranges and fatigue life, for different materials.

When subjected to random excitation, fatigue failure occurs as a result of the com-

Table 2: $R$ and $NMSE$ values for the estimated spectra using equation (27) and the Dynamic Morison model (6)

| Data Set | $R$ | $NMSE$ |
|---|---|---|
| Salford Data Set 1 | 9.98% | 22.77% |
| Salford Data Set 2 | 12.66% | 14.74% |
| Salford Data Set 3 | 6.03% | 16.42% |
| Christchurch Bay Data Set | 9.48% | 16.18% |
| De-Voorst Data Set | 3.91% | 28.86% |

bined effect of stress cycles of many different amplitudes and the S-N curve is not directly applicable. If the random excitation is a narrow band process, in which separate stress cycles can be identified, then Miner's rule can be applied and the fatigue life can be assessed based on the cumulative damage: $\sum \frac{n_i}{N_i} = 1$, where $n_i$ is the number of cycles applied at the stress level $S_i$ and $N_i$ is the number of stress cycles to failure at stress $S_i$.

In the Salford experiments the cylinder was subjected to random waves with a narrow band rectangular spectral density function. The wave force was measured on a small cylindrical element and the input velocity was the ambient horizontal water particle velocity at the mid point of the element (obtained without the cylinder in position).

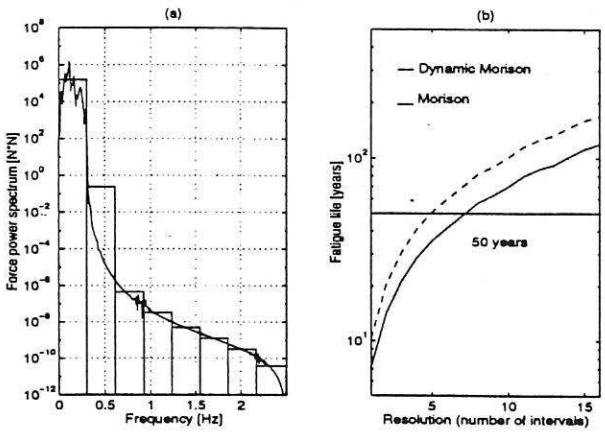


Figure 7: Fatigue life estimation for Christchurch Bay Data Set: (a) The force power spectrum approximation; (b) Fatigue life for Morison (solid line) and Dynamic Morison (dashed line) equations;

The fatigue life will be determined by the stress power spectrum. Different stress amplitudes can be found by using a simple and direct method presented in Osgood (1982). The stress power spectrum is approximated by constant power levels, with identical frequency bandwidth, as presented in Figure 7 (a). The number of cycles to failure is then determined by using the standard S-N curve and the fatigue life computed. In this study

the standard S-N curves for steel, class W are used (British Standards Institution, 1980). The fatigue life values computed for all five data sets and the corresponding spectra from the Figures 1-5 (b)-(f) are presented in Table 3.

Table 3: Fatigue life [years]

| Data Set | Original Output | Smooth Output | NARMAX | Morison | Dynamic Morison |
|---|---|---|---|---|---|
| Salford Data Set 1 | 58.65 | 57.97 | 69.58 | 69.46 | 69.59 |
| Salford Data Set 2 | 117.63 | 120.80 | 135.03 | 134.60 | 135.05 |
| Salford Data Set 3 | 90.78 | 87.61 | 96.71 | 96.40 | 96.71 |
| Christchurch Bay Data Set | 66.42 | 76.92 | 162.22 | 119.29 | 169.05 |
| De-Voorst Data Set | 89.20 | 89.34 | 95.71 | 85.75 | 91.30 |

The precision of the fatigue life approximation will increase with the number of frequency intervals in the stress power spectrum, as shown in Figure 7 (b). On each interval the stress level is considered to be the mean value of stress on that interval and therefore for a small number of frequency intervals the approximated stress level is larger than the original one and the corresponding fatigue life will be shorter.

The fatigue life does not became independent of the number of frequency intervals within the maximum number investigated (16) and Table 3 is only intended to give an indicator of relative magnitudes. Clearly the Morison equation gives a smaller fatigue life as might be expected and this is quite marked for the Christchurch Bay case where nonlinearities are greatest (Stansby et al, 1992).

## 4.4 Spectral analysis for the Morison equation

The analytic expression for the response spectrum (25) allows an easy and simple interpretation of the wave force power spectrum for both the Morison and Dynamic Morison equations.

The response power spectrum for the Dynamic Morison equation has been derived in equation (27) and this can be re-expressed as:

$$S_{FF}(\omega) = S_{uu}(\omega)\left[|H_1(\omega)|^2 + \frac{6}{2\pi}Real(H_1(\omega))Real(H_3(\omega,0,0))\int_{-\infty}^{\infty} S_{uu}(\gamma)d\gamma + \right.$$
$$\left. + \left(\frac{3}{2\pi}\right)^2 |H_3(\omega,0,0)|^2\left(\int_{-\infty}^{\infty} S_{uu}(\gamma)d\gamma\right)^2\right] +$$

$$+ \quad \frac{6}{(2\pi)^2}|H_3(\omega,0,0)|^2 \int_{-\infty}^{\infty}\int_{-\infty}^{\infty} Suu(\omega-\gamma_1-\gamma_2)S_{uu}(\gamma_1)S_{uu}(\gamma_2)d\gamma_1 d\gamma_2$$

$$S_{FF}(\omega) = S_{uu}(\omega)\left|H_1(\omega)+\frac{3k}{2\pi}H_3(\omega,0,0)\right|^2 + \frac{6}{(2\pi)^2}|H_3(\omega,0,0)|^2 \int_{-\infty}^{\infty}\int_{-\infty}^{\infty} Suu(\omega-\gamma_1-\gamma_2)$$
$$S_{uu}(\gamma_1)S_{uu}(\gamma_2)d\gamma_1 d\gamma_2 \tag{31}$$

where the constant $k = \int_{-\infty}^{\infty} S_{uu}(\gamma)d\gamma$.

This equation clearly shows the contribution that the linear and nonlinear terms in the model make to the response power spectrum. A similar expression for the response power spectrum can be found for the Morison equation, considering the frequency response functions derived for equation (3):

$$\begin{aligned} H_1(\omega_1) &= K_{d1} + j\omega_1 K_i \\ H_2(\omega_1,\omega_2) &= 0 \\ H_3(\omega_1,\omega_2,\omega_3) &= K_{d3} \end{aligned} \tag{32}$$

In this case, the third order transfer function $H_3(\omega_1,\omega_2,\omega_3)$ reduces to a constant $K_{d3}$. In this case, the response power spectrum (31) can be simplified in to:

$$\begin{aligned} S_{FF}(\omega) &= S_{uu}(\omega)\left|K_{d1}+j\omega K_i+\frac{3k}{2\pi}K_{d3}\right|^2 + \frac{6}{(2\pi)^2}|K_{d3}|^2 \int_{-\infty}^{\infty}\int_{-\infty}^{\infty} Suu(\omega-\gamma_1-\gamma_2) \\ &\quad S_{uu}(\gamma_1)S_{uu}(\gamma_2)d\gamma_1 d\gamma_2 \\ &= S_{uu}(\omega)|H_1(\omega)|^2 + k_1 S_{uu}(\omega) + k_2 \int_{-\infty}^{\infty}\int_{-\infty}^{\infty} Suu(\omega-\gamma_1-\gamma_2) \\ &\quad S_{uu}(\gamma_1)S_{uu}(\gamma_2)d\gamma_1 d\gamma_2 \end{aligned} \tag{33}$$

where $k_1 = \frac{6}{2\pi}K_{d1}K_{d3}\int_{-\infty}^{\infty} S_{uu}(\gamma)d\gamma + \left(\frac{3}{2\pi}K_{d3}\int_{-\infty}^{\infty} S_{uu}(\gamma)d\gamma\right)^2$

$k_2 = \frac{6}{(2\pi)^2}K_{d3}^2$

The first term $term_1 = S_{uu}(\omega)|H_1(\omega)|^2$ in equation (33) represents the contribution of the linear terms in equation (3). The second term $term_2 = k_1 S_{uu}(\omega)$ is a fraction of the input spectrum and the third term $term_3 = k_2 \int_{-\infty}^{\infty}\int_{-\infty}^{\infty} Suu(\omega-\gamma_1-\gamma_2)S_{uu}(\gamma_1)S_{uu}(\gamma_2)d\gamma_1 d\gamma_2$ is the third order convolution applied to the input spectrum respectively. These terms were estimated for the Salford Data Set 1 and are illustrated in Figure 8.

Figure 8 shows that the main contribution to the response spectrum is generated by the linear terms, especially at high frequencies. Any linear frequency function $H_1(\omega)$,

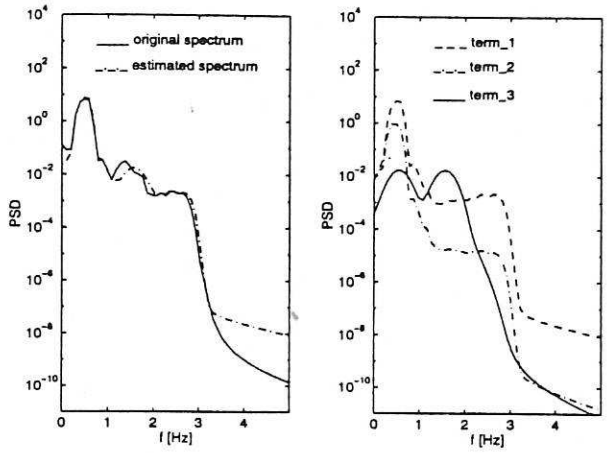


Figure 8: The force power spectrum for the Morison equation - Data Set 1 (33)

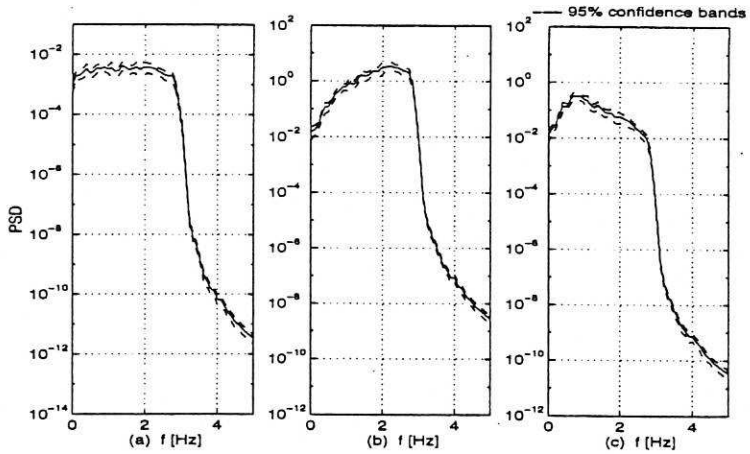


Figure 9: The force power spectrum for (a) high frequency input applied to (b) Morison and (c) Dynamic Morison equations - Data Set 1

for which $\lim_{\omega\to\infty} |H_1(\omega)| = \infty$, will produce a response spectrum with the same behaviour: $\lim_{\omega\to\infty} S_{FF}(\omega) = \infty$. For example, when a high frequency input wave with a very small amplitude (Figure 9 (a)) is applied to the Morison model, the force spectrum increases as shown in Figure 9 (b).

This can have critical consequences on the fatigue design for offshore structures in which the stress is directly proportional to the wave force amplitude. Therefore the stress $S$ is expected to increase infinitely $\lim_{\omega\to\infty} S = \infty$ and therefore the number of cycles before failure $\lim_{\omega\to\infty} N = 0$. Consequently the offshore structure will tend to be grossly over engineered.

For Dynamic Morison model (Figure 9 (c)) the spectrum is not dominated by the linear transfer function at high frequencies and therefore it is expected to provide an improved and more reliable estimate of the fatigue life for offshore structures. Therefore, the

estimated fatigue life in section 4.3 for the Dynamic Morison equation is longer than the corresponding value found for the Morison equation, as it can be seen in Figure 7 (b) and Table 3.

# 5 Conclusions

An expression for the output spectrum of nonlinear wave forces has been derived based on the higher order frequency response functions and properties of the input. It was shown how this can be evaluated for the Dynamic Morison and Morison equations to reveal the explicit dependence of the spectra on the coefficients in the nonlinear differential equation. An analysis and interpretation of the Morison equation response spectrum was also presented.

Similar results can easily be derived for other nonlinear differential equations or difference (NARMAX) equation models by evaluating the higher order frequency response functions for these and substituting them into the expression for the output spectrum.

These results provide a unique insight by explicitly showing how the time-domain coefficients influence the output spectra and vice versa. Application of the results was demonstrated using five data sets from Salford, De-Voorst and Christchurch Bay. An example was given of how fatigue life is affected by use of the conventional Morison equation rather than more correct Dynamic Morison equation.

# References


[1] Morison, J.R., O'Brien, M.P., Johnson, J.W. and Schaf, S.A., 1950, "The force exerted by surface waves on piles", Petroleum Transactions, No.189, pp.189-202.

[2] Stansby, P.K., Worden, K., Billings, S.A., Tomlinson, G.R., 1992, "Improved wave force classification using system identification", Applied Ocean Research, No.14, pp.107-118.

[3] Worden, K., Stansby, P.K., Tomlinson, G.R., Billings, S.A., 1994, "Identification of nonlinear wave forces", Journal of Fluids and Structures, No.8, pp.19-71.

[4] Swain, A.K., Billings, S.A., Stansby, P.K., Baker, M., 1996, "Accurate prediction of nonlinear wave forces: Part I (Fixed cylinder)", submitted for publication.

[5] Volterra, V., 1959, "Theory of functionals and of integral and integro-differential equations", New York: Dover, pp.4.

[6] Rugh, W.J., 1981, "Nonlinear systems theory - The Volterra/Wiener approach", The Johns Hopkins Press Ltd., London, pp.213-223.

[7] Peyton-Jones, J.C. and Billings, S.A., 1990, "Mapping non-linear integro-differential equations into the frequency domain", International Journal of Control, Vol.52, No.4, pp.863-879.

[8] Weigend, S.A. and Gershenfeld, N.A., 1993, "Time series prediction: Forecasting the future and understanding the past", Proc. of the NATO Advanced Research Workshop on Comparative Time Series Analysis, Proc. vol. XV, Addison-Wesley.

[9] Wellstead, P.E., 1986, "Spectral analysis and its applications", Lecture Notes in Control and Information Sciences: Signal Processing for Control, Springer-Verlag, pp.210-245.

[10] Chrysostomos, L.N., Petropulu, A.P., 1993, "Higher-order spectra analysis", Prentice Hall, Englewood Cliffs, New Jersey.

[11] Palm, G., Poggio, T., 1987, "The Volterra representation and the Wiener expansion: validity and pitfalls", SIAM Journal on Applied Mathematics, No.33, pt-2.

[12] Leontaritis, I.J., Billings, S.A., 1985, "Input-output parametric models for nonlinear systems; Part 1: deterministic nonlinear systems", International Journal of Control, No.41, pp.303-328.

[13] Bendat, J.S. and Piersol, A.G., 1986, "Decomposition of wave forces into linear and non-linear components", Journal of Sound and Vibration, Vol.106, No.3, pp.391-408.

[14] Proakis, J.G., Rader, C.M., Ling, F., Nikias, C.L., 1992, "Advanced digital signal processing", Macmillan, New York.

[15] Baker, M., 1994, "Wave loading on a small diameter flexibly mounted cylinder in random waves", Ph.D. Dissertation, University of Salford.

[16] Osgood, C.C., 1982, "Fatigue design", Pergamon Press.

[17] Korenberg, M., Billings, S.A., Liu, Y.P., McIlloy, P.I., 1988, "Orthogonal parameter estimation algorithm for non-linear stochastic systems", International Journal of Control, Vol.48, No.1, pp.193-210.

[18] British Standards Institution, 1980, "Steel, concrete and composite bridges. Part 10: Code of practice for fatigue", BS 5400, BSI, London.